GEOPHYSICS

Seismic potential of weak, near-surface faults revealed at plate tectonic slip rates

Matt J. Ikari* and Achim J. Kopf

The near-surface areas of major faults commonly contain weak, phyllosilicate minerals, which, based on laboratory friction measurements, are assumed to creep stably. However, it is now known that shallow faults can experience tens of meters of earthquake slip and also host slow and transient slip events. Laboratory experiments are generally performed at least two orders of magnitude faster than plate tectonic speeds, which are the natural driving conditions for major faults; the absence of experimental data for natural driving rates represents a critical knowledge gap. We use laboratory friction experiments on natural fault zone samples at driving rates of centimeters per year to demonstrate that there is abundant evidence of unstable slip behavior that was not previously predicted. Specifically, weak clay-rich fault samples generate slow slip events (SSEs) and have frictional properties favorable for earthquake rupture. Our work explains growing field observations of shallow SSE and surface-breaking earthquake slip, and predicts that such phenomena should be more widely expected.

INTRODUCTION

Identifying areas that are at risk of earthquake damage, either directly or indirectly from associated tsunamis or landslides, requires a reasonable expectation of how major faults in a particular region are expected to slip (*1*). Many long-standing tenets of fault and earthquake mechanics are based on an assumption that stronger materials are associated with slip instability responsible for earthquake generation. In particular, in Kanamori's (*2*) asperity model of earthquake rupture, the strong fault portions (asperities) rupture during earthquakes and generate high-frequency radiation, whereas regions associated with postseismic creep are designated as weak. This is supported by laboratory friction experiments showing that weak materials such as phyllosilicate minerals (that is, clays and micas) tend to suppress stick-slip behavior (*3*, *4*) and also exhibit velocity-strengthening frictional behavior (that is, an increase in strength in response to faster driving) (*5*), which is favorable for stable fault creep (*6*). Combined with seismologic observations, this has led to the development of the "seismogenic zone" model, in which earthquake nucleation occurs at a depth of several kilometers rather than extending to the Earth's surface in most cases (*7*, *8*). Above the seismogenic zone, shallow aseismic behavior is associated with initially weak, unconsolidated sediments that require diagenetic transformation (and associated strengthening) before seismogenesis is possible at greater depth, as indicated by laboratory experiments (*9*, *10*). In the field, the discovery of the extremely weak mineral smectite in the central San Andreas Fault in California has been used to explain why this portion of the fault creeps (*11*).

However, despite the widespread acceptance of the asperity model and seismogenic zone model, several recent observations raise doubts concerning their general applicability. For example, great M_w (moment magnitude) ~9 earthquakes such as the 2011 Tohoku event demonstrated that coseismic slip can propagate all the way to the trench (*12*), through material considered to be "aseismic" (*13*). Shallow slow earthquakes have been observed within accretionary prisms (*14*), and also on the central San Andreas Fault (*15*, *16*), suggesting that weak, clay-dominated fault regions should not necessarily be classified as "stable."

It is important to recognize that the established framework for understanding fault slip behavior is primarily based on experimental studies performed at driving velocities of ~10^{-7} to 10^{-4} m/s (or roughly within a range of micrometers to millimeters per second). This is too fast to simulate plate convergence rates of several centimeters per year (*17*) or on the order of ~10^{-9} m/s (in the range of nanometers per second). Similarly, many long-duration slow slip events (SSEs) exhibit slip velocities that are lower than 10^{-7} m/s (*18*) and therefore cannot be replicated by standard friction experiments. Surprisingly little information has been obtained through friction experiments where the slip velocity is slower than ~10^{-7} m/s, and only for analog materials such as granite, calcite, halite, or halite/muscovite mixtures (*19*–*21*) rather than natural fault gouges. However, plate convergence velocities are perhaps the most important factor controlling fault slip behavior because they represent the boundary condition for slip on plate boundary faults.

Here, we investigate the frictional behavior of natural fault zone materials recovered by scientific drilling projects targeting subduction zones [Japan Trench (*22*), Nankai Trough (*23*, *24*), Costa Rica (*25*), Barbados (*26*), and Cascadia (*27*)], continental strike-slip faults [San Andreas Fault (*28*) and Alpine Fault (*29*)], and a detachment normal fault [Woodlark Basin (*30*)] (Fig. 1). All samples were recovered from a depth of less than 1 km, except the San Andreas Fault sample (~2.7 km); therefore, we tested our samples at 20°C and 10 MPa effective normal stress to approximate the in situ condition (table S1). Following Ikari *et al.* (*31*, *32*), shearing was performed on powdered samples mixed with a 3.5% NaCl brine in a single–direct shear configuration to measure the coefficient of sliding friction $\mu = \tau/\sigma_n'$, where τ is the shear strength and σ_n' is the effective normal stress. In our tests, we sheared the samples at 10 μm/s for 4 to 5 mm to establish steady-state shear geometry and residual friction level, and then decreased the slip velocity to a value ranging from 5.3 to 8.5 cm/year (1.7 to 2.7 nm/s) for at least 2 mm, thus simulating realistically slow tectonic driving velocities (see the Supplementary Materials). We then increased the velocity by a factor of 3 to determine the dependence of friction on driving velocity. For comparison, we also conducted a set of experiments with velocity steps at higher slip velocities commonly used in typical friction experiments. We evaluate all changes in slip velocity in our experiments and consider them in three groups: (i) a decrease from the initial rate of 10 μm/s to rates of centimeters per year and a threefold increase from rates of centimeters per year; (ii) a decrease from 10 to 0.1 μm/s and increases from 0.1 to 0.3 μm/s and 0.3 to 1 μm/s; and

MARUM—Center for Marine Environmental Sciences and Faculty of Geosciences, University of Bremen, Bremen, Germany.
*Corresponding author. Email: mikari@marum.de

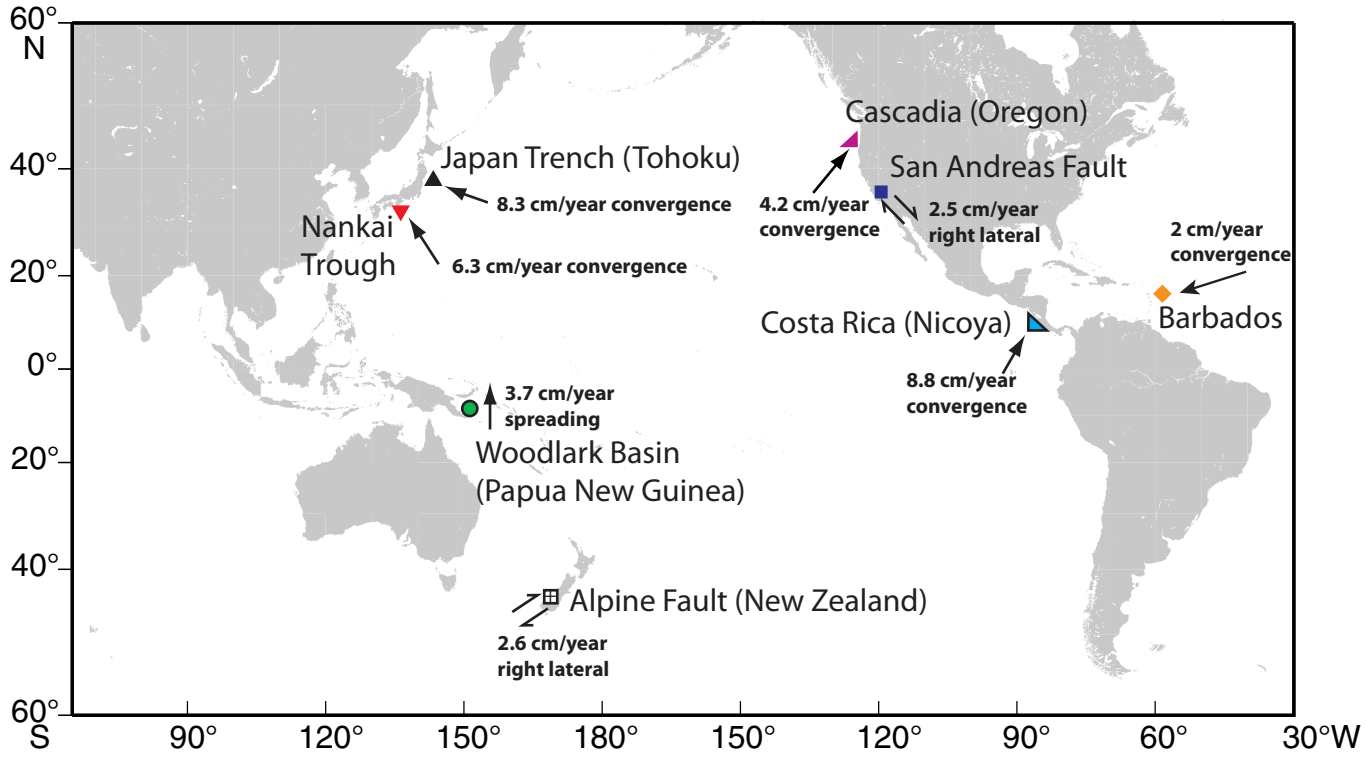

Fig. 1. Study areas. World map showing the locations of scientific drilling where the samples tested in this study were recovered. Triangles/diamond, subduction thrusts; squares, transform faults; circle, normal fault. See the Supplementary Materials for references pertaining to geologic rates. Map courtesy of the International Ocean Discovery Program JOIDES Resolution Science Operator.

(iii) increases from 1 to 3 μm/s, 3 to 10 μm/s, and 10 to 30 μm/s. The dependence of friction on velocity is evaluated with the parameter $a\text{-}b = (\mu_o - \mu)/\ln(V/V_o)$, where μ_o is the steady-state friction coefficient at an initial velocity V_o and μ is the steady-state friction coefficient at a final velocity V (*33*). In most cases, we use an inverse modeling technique (*34*) to determine *a-b*. As applied to fault slip, positive *a-b* ("velocity strengthening") is favorable for stable fault creep, whereas negative *a-b* ("velocity weakening") is a requirement for frictional instability and therefore favorable for earthquake slip (*6*, *33*).

RESULTS

We observe that when V = 1 to 30 μm/s, velocity-strengthening friction is mostly observed except in the stronger samples (Cascadia and Alpine Fault), and an inverse relationship between fault strength and *a-b* is observed, consistent with an earlier work (*5*) (Fig. 2). At lower driving velocities of 0.1 to 1 μm/s, a mix of positive and negative *a-b* values is observed. When plate tectonic rates of centimeters per year are used, velocity-weakening friction is mostly observed and occurs for every sample except the Woodlark Basin and the San Andreas Fault, even though friction coefficients (considering here μ_o) range as low as 0.15. Our data demonstrate that under naturally slow driving rates, weak materials from natural fault zones exhibit a tendency for unstable slip, which is not recognized in typical laboratory experiments and previously only seen in a few studies using generally stronger materials (granite, calcite, and halite) as fault gouge analogs (*19*, *20*).

Velocity-weakening friction, however, is not the only indicator of unstable slip. Under constant driving at slip rates of centimeters per year, several of the gouges in this study also exhibited strength perturbations interpreted to be experimentally observed SSE. Such perturbations are characterized by a stress drop concurrent with a measureable increase in the sample slip velocity (*31*). In most cases, these slow events are only observed at the lowest sliding velocity (that is, at plate rates). However, SSE also appeared during shear at slightly higher velocities for samples from the Woodlark Basin (16 cm/year), Barbados (16 and 40 cm/year), and the San Andreas Fault (25 cm/year). SSEs in the San Andreas Fault sample were only observed at 25 cm/year, and not at slower rates of 5 or 16 cm/year. SSE stress drops range from 20 to 870 kPa, and peak slip velocities range from 8 to 84 cm/year. The data set as a whole shows that events with larger stress drops tend to reach higher peak slip velocities (Fig. 3), a phenomenon also observed in recent laboratory studies targeting frictional stability transitions in fault gouge (*35*, *36*), and is thus consistent with SSEs being slow frictional instabilities.

DISCUSSION

The appearance of frictional instability at very slow driving rates suggests that it arises from a process that occurs over time scales much longer than the duration of typical laboratory experiments. For fault gouge, in general, time-dependent plastic deformation at grain-scale asperity contacts drives strengthening via growth in real areas of contact; if the slip velocity increases, this growth mechanism is more limited because of faster replacement of contacts, causing the fault to be weaker at the higher velocity, resulting in velocity-weakening friction (*33*). At typical intermediate shearing velocities, time-dependent strengthening

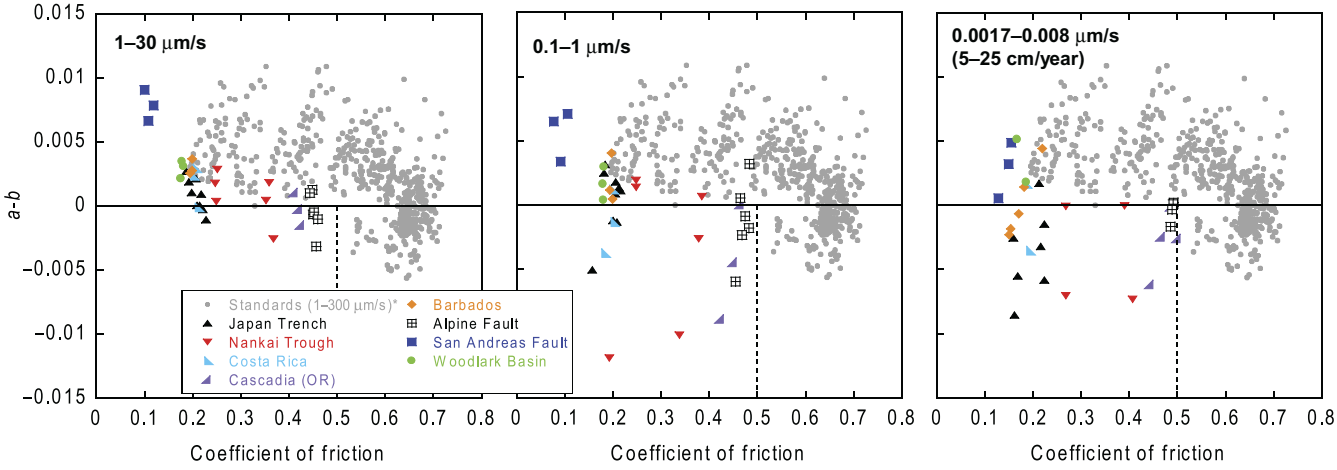

Fig. 2. Frictional properties. Velocity-dependent friction parameter *a-b* as a function of the coefficient of friction immediately preceding the velocity change. Data for standards from Ikari *et al.* (*5*) and Japan Trench data from Ikari *et al.* (*31*, *32*). Symbols and colors follow those in Fig. 1.

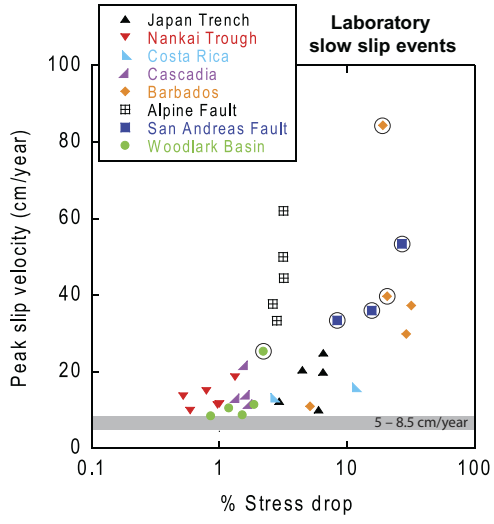

Fig. 3. Experimental SSE characteristics. Peak slip velocity as a function of % stress drop for laboratory-generated SSE. Circled data points indicate SSE generated at slip rates higher than 8.5 cm/year (see table S1 for details). Symbols and colors follow those in Figs. 1 and 2. Japan Trench data from Ikari *et al.* (*31*).

rates (or "frictional healing" rates) are significantly larger for strong framework minerals compared to weak phyllosilicates (*37*). Recent experiments using the same smectite-rich San Andreas Fault gouge tested here demonstrated that advanced healing appears at much longer time scales (on the order of days) compared to typical friction experiments (*38*). Thus, extremely slow slip rates are required to allow advanced healing during shear, which causes velocity weakening in weak, phyllosilicate-rich faults.

The velocity-weakening frictional behavior of our gouges likely produces the laboratory SSE we observe. Several of our study areas exhibit both laboratory and natural SSEs, which occur shallower than a depth of few kilometers and hence would be outside the seismogenic zone. This includes a shallow (~6 km) SSE offshore Costa Rica (*39*), tremor activity associated with slow slip off the central/southern coast of Oregon (*40*), SSE at a depth of <4 km on both the northern (*16*) and southern (*15*) ends of the San Andreas Fault creeping section, and low-frequency earthquakes (a faster form of slow slip) within the accretionary prism in the Nankai subduction zone (*14*). Two large SSEs were observed before the 2011 Tohoku earthquake within the eventual rupture area, demonstrating that SSE and ordinary earthquakes can occur on the same fault patch (*41*). Our laboratory data suggest that SSEs can be considered frictional instabilities; therefore, their occurrence is diagnostic of unstable fault portions.

The unstable nature of the fault gouges we demonstrate here could facilitate the propagation of coseismic rupture and slip at shallow depths, because the velocity-weakening property we observe at very low rates allows stress drops and energy release (*6*). We note that the velocity weakening we observe does not necessarily guarantee the occurrence of coseismic rupture, which is controlled by several other factors such as the energetics of a rupture propagating from elsewhere on the fault (*42*), the preexisting shear stress level on the fault (*43*), the dynamic behavior of the material at high (centimeters to meters per second) slip velocities (*13*), and the elastic properties of the fault surroundings (*6*, *33*, *35*). In some cases, velocity-strengthening friction at intermediate rates may be expected to resist rupture propagation by acting as an energy sink so that instabilities nucleating on the shallow portions of faults may be arrested earlier, resulting in the occurrence of shallow SSE rather than ordinary earthquakes (*44*, *45*). The question of what specific conditions cause fault instability to eventually result in coseismic slip warrants further study; however, the common occurrence of SSE and velocity-weakening friction at slip rates of centimeters per year in our laboratory experiments reveals the possibility of such instability. This newly recognized ability of shallow faults, including weak faults containing phyllosilicate minerals, to host earthquake slip should be a consideration worldwide.

MATERIALS AND METHODS

For this study, we tested 10 natural samples, all obtained from fault zones by scientific drilling (table S1). The samples were tested as powdered gouges and prepared by air drying fragments of the whole-round core, which were then crushed with a mortar and pestle to a grain size of

<125 μm. Data from samples from the Tohoku region of the Japan Trench, tested as intact cylinders trimmed from whole-round cores, reported by Ikari *et al.* (*31*) were also included. The powders were then mixed with simulated seawater (3.5% NaCl brine) into a stiff paste and cold-pressed into the sample cell, which houses a cylindrical volume (25 mm in diameter, 30 mm in height) within two stacked steel plates. The brine was also used for the nonmarine transform fault samples (San Andreas and Alpine faults) for consistency and also because the San Andreas Fault pore fluid contains a significant amount of ions (*46*). The sample cell was flooded with seawater and thus tested in a fluid-saturated condition. The samples were confined by the sample cell and were not jacketed. All tests were performed in a climate-controlled room at a constant temperature of 20°C.

For our experiments, we used a GIESA RS5 direct shear apparatus (fig. S1A) (*31*, *32*). Constant normal stress was applied to the top face of the sample with a vertical piston, controlled by a servo system with a proportional-integrative-derivative controller. We applied a normal stress of 10 MPa, appropriate for our samples that were recovered from depths of <1 km, with the exception of the San Andreas Fault sample that was recovered from a depth of ~2.7 km (table S1). The samples were then consolidated until the change in sample height over time became negligible. The time allowed for consolidation was at least overnight (~18 hours) and, in some cases, several days. The sample was allowed to drain at the top and bottom faces via porous metal frits; the top is open to the atmosphere and the bottom to an open pore fluid reservoir within which the sample cell sits to prevent desiccation. Although we did not directly control the pore pressure, we sheared the samples only after the sample height was constant and assumed that any excess pore pressure that may have developed during loading dissipated during the consolidation process. Therefore, in our experiments, we assumed that the applied stress equaled the effective normal stress (10 MPa) acting on the sample (pore pressure = 0). The data from Ikari *et al.* (*31*, *32*) for the Tohoku sample were obtained at an effective normal stress of 7 MPa. We further assumed that because the sample maintained zero pore pressure during the experiment, the frictional behavior we observed was not attributable to fluctuations in pore fluid pressure.

To induce deformation, the lower plate was displaced horizontally relative to the top plate by an electric motor, inducing planar (that is, localized) shear within the sample. The shear load was corrected for the shear resisting force of the interface between the two plates of ~9 N. For our samples, which have an area of 5.07×10^{-4} m^2, the resolution of the load cells is 0.30 kPa in normal stress and 0.15 kPa in shear stress. Fluctuations due to electrical noise were estimated to be ±~0.4 μm in displacement and ±~2 kPa in load. We used two potentiometric displacement sensors with a resolution of 0.8 μm (Fig. 1). The first sensor measures displacement directly at the sample cell, which represents the shear displacement of the sample without effects of apparatus stiffness. The second sensor measures displacement at the horizontal load cell (that is, the loading point displacement). By using the two sensors, we may (i) observe apparatus stiffness effects and (ii) confirm that the observed shear perturbations are occurring in the sample, rather than being artifacts of the driving apparatus. We measured the horizontal stiffness to be 3.8 kN/mm under a normal stress of 7 MPa; the stiffness of the apparatus was not modified for these experiments. The driving mechanism uses a stepper motor with an update rate of 0.19 Hz and a step width of 0.015 μm, which produces a minimum time-averaged displacement rate of 1.7 nm/s.

We measured the shear strength τ throughout the experiment, which we used to calculate an apparent friction coefficient μ

$$\mu = \frac{\tau}{\sigma_n'} \tag{1}$$

We considered the shear stress as one entity and did not distinguish between the cohesive and frictional portions of the shear strength. The velocity dependence of friction, measured as the frictional response to a step change in velocity, is described by the relations

$$\mu = \mu_o + a \ln\left(\frac{V}{V_o}\right) + b_1 \ln\left(\frac{V_o \theta_1}{D_{c1}}\right) + b_2 \ln\left(\frac{V_o \theta_2}{D_{c2}}\right) \tag{2}$$

$$\frac{d\theta_i}{dt} = 1 - \frac{V\theta_i}{D_{ci}}, i = 1, 2 \tag{3}$$

where a, b_1, and b_2 are dimensionless constants; θ_1 and θ_2 are state variables (units of time); and D_{c1} and D_{c2} are critical slip distances over which friction evolves to a new steady-state value (*33*, *47*). If the data are well described by a single state variable, then $D_{c1} = D_{c2}$ and we take $b_2 = 0$. To account for the possibility of one or two state variables, we defined $b = b_1 + b_2$. Equation 3 is known as the "Dieterich" or "slowness" law, which describes the evolution of the state variable θ. Although other laws may be used, we chose this law because it describes how friction can change as a function of time even in the limiting case of zero slip velocity, which has been verified experimentally (*33*). The individual RSF (rate- and state-friction) parameters a, b_1, b_2, D_{c1}, and D_{c2} were determined by inverse modeling using an iterative least-squares method that also accounts for elastic interaction with the testing machine by incorporating an expression for the system stiffness k (friction/displacement) (*34*)

$$\frac{d\mu}{dt} = k(V_{lp} - V) \tag{4}$$

Conventionally, $(V_{lp} - V)$ is defined as the difference between true fault slip velocity V and the remotely recorded load point velocity V_{lp}. The apparatus stiffness k includes the forcing blocks and support structure, and also the sample itself. For our apparatus stiffness (3.8 kN/mm) and sample dimensions (5×10^{-4} m^2), k = ~1 mm^{-1}. The modeling procedure described here also allows the removal of long-term slip-dependent friction trends to avoid biasing and more accurately determine the friction velocity dependence (*47*). An example of experimental friction data for a velocity step and the inverse model are shown in fig. S1B.

Although the modeling technique is a more robust method for determining *a-b*, it is difficult to apply to large, negative velocity differences and therefore was not used for the decrease from the background velocity to plate tectonic velocities. In these cases, we measure the difference in steady-state friction before and after the velocity step as $\Delta\mu_{ss} = \mu_o - \mu$ and use a reduced form of Eqs. 2 and 3 to calculate the velocity dependence of friction as

$$a\text{-}b = \frac{\Delta\mu_{ss}}{\Delta \ln V} \tag{5}$$

An example of an *a-b* value determined by this method is shown in fig. S1C. Determination of "steady state" is an approximation by which

no obvious slip-hardening or weakening trends are present where the measurement is made. In cases where a clearly linear slip-dependent trend is superimposed on the data, this trend may be removed by applying a constant correction factor (*47*).

Where SSEs were observed, we measured the stress drop $\Delta\tau$ from the shear stress record. SSEs were confirmed by the occurrence of a distinct increase in slip displacement, and thus slip velocity, in the sample concurrent with the stress drop (fig. S2). Comparison between sample displacement and sample slip velocity with records of the load point displacement and load point velocity shows that the perturbations are only observed at the sample and not at the load cell; this confirms that the SSEs are occurring in the sample and are not an artifact of the apparatus.

SUPPLEMENTARY MATERIALS

Supplementary material for this article is available at http://advances.sciencemag.org/cgi/content/full/3/11/e1701269/DC1

fig. S1. Experimental apparatus and examples of experimental data.
fig. S2. Time series of experimental friction data for a sample from the Cascadia subduction zone (experiment B565) showing details of an experimentally observed SSE.
table S1. Sample and sample location details.
table S2. Velocity-dependent friction parameters determined by inverse modeling.
table S3. Velocity dependence of friction determined by direct measurement.
table S4. Experimentally measured SSE parameters.
References (*48*–*50*)

REFERENCES AND NOTES

1. C. H. Scholz, Paradigms or small change in earthquake mechanics. *Int. Geophys.* **51**, 505–517 (1992).
2. H. Kanamori, Rupture process of subduction-zone earthquakes. *Annu. Rev. Earth Planet. Sci.* **14**, 293–322 (1986).
3. T. Shimamoto, J. M. Logan, Effects of simulated clay gouges on the sliding behavior of Tennessee sandstone. *Tectonophysics* **75**, 243–255 (1981).
4. N. M. Beeler, Laboratory-observed faulting in intrinsically and apparently weak materials: Strength, seismic coupling, dilatancy and pore-fluid pressure, in *The Seismogenic Zone of Subduction Thrust Faults* (Columbia Univ. Press, 2007), pp. 370–449.
5. M. J. Ikari, C. Marone, D. M. Saffer, On the relation between fault strength and frictional stability. *Geology* **39**, 83–86 (2011).
6. C. H. Scholz, Earthquakes and friction laws. *Nature* **391**, 37–42 (1998).
7. R. D. Hyndman, M. Yamano, D. A. Oleskevich, The seismogenic zone of subduction thrust faults. *Isl. Arc* **6**, 244–260 (1997).
8. J. C. Moore, D. Saffer, Updip limit of the seismogenic zone beneath the accretionary prism of southwest Japan: An effect of diagenetic to low-grade metamorphic processes and increasing effective stress. *Geology* **29**, 183–186 (2001).
9. C. Marone, C. H. Scholz, The depth of seismic faulting and the upper transition from stable to unstable slip regimes. *Geophys. Res. Lett.* **15**, 621–624 (1988).
10. S. Trütner, A. Hüpers, M. J. Ikari, A. Yamaguchi, A. J. Kopf, Lithification facilitates frictional instability in argillaceous subduction zone sediments. *Tectonophysics* **665**, 177–185 (2015).
11. A. M. Schleicher, B. A. van der Pluijm, L. N. Warr, Nanocoatings of clay and creep of the San Andreas Fault at Parkfield, California. *Geology* **38**, 667–670 (2010).
12. T. Fujiwara, S. Kodaira, T. No, Y. Kaiho, N. Takahashi, Y. Kaneda, The 2011 Tohoku-Oki earthquake: Displacement reaching the trench axis. *Science* **334**, 1240 (2011).
13. D. R. Faulkner, T. M. Mitchell, J. Behnsen, T. Hirose, T. Shimamoto, Stuck in the mud? Earthquake nucleation and propagation through accretionary forearcs. *Geophys. Res. Lett.* **38**, L18303 (2011).
14. Y. Ito, K. Obara, Dynamic deformation of the accretionary prism excites very low frequency earthquakes. *Geophys. Res. Lett.* **33**, L02311 (2006).
15. N. R. Goulty, R. Gilman, Repeated creep events on the San Andreas Fault near Parkfield, California, recorded by a strainmeter array. *J. Geophys. Res.* **83**, 5415–5419 (1978).
16. A. T. Linde, M. T. Gladwin, M. J. S. Johnston, R. L. Gwyther, R. G. Bilham, A slow earthquake sequence on the San Andreas Fault. *Nature* **383**, 65–68 (1996).
17. C. DeMets, R. G. Gordon, D. F. Argus, Geologically current plate motions. *Geophys. J. Int.* **181**, 1–80 (2010).
18. S. Ide, G. C. Beroza, D. R. Shelly, T. Uchide, A scaling law for slow earthquakes. *Nature* **447**, 76–79 (2007).
19. J. D. Weeks, Constitutive laws for high-velocity frictional sliding and their influence on stress drop during unstable slip. *J. Geophys. Res.* **98**, 17637–17648 (1993).
20. T. Shimamoto, Transition between frictional slip and ductile flow for halite shear zones at room temperature. *Science* **231**, 711–714 (1986).
21. A. R. Niemeijer, C. J. Spiers, Velocity dependence of strength and healing behaviour in simulated phyllosilicate-bearing fault gouge. *Tectonophysics* **427**, 231–253 (2006).
22. F. M. Chester, J. Mori, N. Eguchi, S. Toczko; Expedition 343/343T Scientists, Japan Trench Fast Drilling Project (JFAST). *Proc. IODP* **343/343T** (2013).
23. G. F. Moore, A. Taira, A. Klaus, K. Becker, L. Becker, B. Boeckel, B. A. Cragg, P. A. Dean, C. L. Fergusson, P. Henry, S. Hirano, T. Hisamitsu, S. Hunze, M. Kastner, A. J. Maltman, J. K. Morgan, Y. Murakami, D. M. Saffer, M. Sánchez-Gómez, E. J. Screaton, D. C. Smith, A. J. Spivack, J. Steurer, H. J. Tobin, K. Ujiie, M. B. Underwood, M. Wilson, Deformation and fluid flow processes in the Nankai Trough accretionary prism. *Proc. ODP Init. Rep.* **190** (2001).
24. M. Kinoshita, H. Tobin, J. Ashi, G. Kimura, S. Lallemant, E. J. Screaton, D. Curewitz, H. Masago, K. T. Moe; Expedition 314/315/316 Scientists, NanTroSEIZE Stage 1: Investigations of seismogenesis, Nankai Trough, Japan. *Proc. IODP* **314/315/316** (2009).
25. G. Kimura, E. A. Silver, P. Blum, G. Blanc, A. Bolton, M. Clennell, J. R. Griffin, B. Housen, M. Ibaraki, T. Kanamatsu, M. Kastner, N. Lindsley-Griffin, A. Lueckge, K. McIntosh, M. Meschede, J. Morris, J. Muza, G. Myers, M. Protti, O. Saether, S. Saito, D. Scholl, G. Spence, H. Tobin, P. Vannucchi, L. White, Costa Rice accretionary wedge sites, 1039–1043. *Proc. ODP Init. Rep.* **170** (1997).
26. T. H. Shipley, Y. Ogawa, P. Blum, J. Ashi, W. Brückmann, F. Filice, A. Fisher, D. Goldberg, P. Henry, B. Housen, M.-J. Jurado, M. Kastner, P. Labaume, T. Laier, E. C. Leitch, A. J. Maltman, A. Meyer, G. F. Moore, J. C. Moore, S. Peacock, A. Rabaute, T. H. Steiger, H. J. To, Northern Barbados Ridge sites, 947–949. *Proc. ODP Init. Rep.* **156** (1995).
27. G. K. Westbrook, B. Carson, R. J. Musgrave, J. Ashi, B. Baranov, K. M. Brown, A. Camerlenghi, J.-P. Caulet, N. Chamov, M. B. Clennell, B. A. Cragg, P. Dietrich, J.-P. Foucher, B. Foucher, M. Hovland, R. D. Jarrard, M. Kastner, A. Kopf, M. E. MacKay, C. Moore, K. Moran, R. J. Parkes, J. Sample, T. Sato, E. J. Screaton, H. J. Tobin, M. J. Whiticar, S. D. Zellers, Cascadia Margin sites, 888–892. *Proc. ODP Init. Rep.* **146** (1994).
28. M. Zoback, S. Hickman, W. Ellsworth; the SAFOD Science Team, Scientific drilling into the San Andreas Fault Zone—An overview of SAFOD's first five years. *Sci. Drill.* **11**, 14–28 (2011).
29. V. G. Toy, C. J. Boulton, R. Sutherland, J. Townend, R. J. Norris, T. A. Little, D. J. Prior, E. Mariani, D. Faulkner, C. D. Menzies, H. Scott, B. M. Carpenter, Fault rock lithologies and architecture of the central Alpine Fault, New Zealand, revealed by DFDP-1 drilling. *Lithosphere* **L395-1** (2015).
30. B. Taylor, P. Huchon, A. Klaus, S. A. M. Awadallah, C. K. Brooks, B. Célérier, E. H. DeCarlo, J. Floyd, G. M. Frost, V. Gardien, S. Gerbaudo, A. M. Goodliffe, J. K. Haumu, N. Ishikawa, G. D. Karner, P. M. Kia, A. Kopf, K. S. Lackschewitz, R. Laronga, B. Le Gall, I. D. Mather, B. D. Monteleone, A. H. F. Robertson, R. C. B. Perembo, J. M. Resig, E. J. Screaton, T. R. Sharp, W. G. Siesser, S. C. Stover, K. Takahashi, P. Wellsbury, Active continental extension in the Western Woodlark Basin, Papua New Guinea. *Proc. ODP Init. Rep.* **180** (1999).
31. M. J. Ikari, Y. Ito, K. Ujiie, A. J. Kopf, Spectrum of slip behaviour in Tohoku fault zone samples at plate tectonic slip rates. *Nat. Geosci.* **8**, 870–874 (2015).
32. M. J. Ikari, J. Kameda, D. M. Saffer, A. J. Kopf, Strength characteristics of Japan Trench borehole samples in the high-slip region of the 2011 Tohoku-Oki earthquake. *Earth Planet. Sci. Lett.* **412**, 35–41 (2015).
33. J. H. Dieterich, Constitutive properties of faults with simulated gouge, in *Mechanical Behavior of Crustal Rocks: The Handin Volume* (American Geophysical Union, 1981), pp. 103–120.
34. L. A. Reinen, J. D. Weeks, Determination of rock friction constitutive parameters using an iterative least squares inversion method. *J. Geophys. Res.* **98**, 15937–15950 (1993).
35. J. R. Leeman, D. M. Saffer, M. M. Scuderi, C. Marone, Laboratory observations of slow earthquakes and the spectrum of tectonic fault slip modes. *Nat. Commun.* **7**, 11104 (2016).
36. M. M. Scuderi, C. Marone, E. Tinti, G. Di Stefano, C. Collettini, Precursory changes in seismic velocity for the spectrum of earthquake failure modes. *Nat. Geosci.* **9**, 695–700 (2016).
37. B. M. Carpenter, M. J. Ikari, C. Marone, Laboratory observations of time-dependent frictional strengthening and stress relaxation in natural and synthetic fault gouges. *J. Geophys. Res. Solid Earth* **121**, 1183–1201 (2016).
38. M. J. Ikari, B. M. Carpenter, C. Vogt, A. J. Kopf, Elevated time-dependent strengthening rates observed in San Andreas Fault drilling samples. *Earth Planet. Sci. Lett.* **450**, 164–172 (2016).
39. K. C. Outerbridge, T. H. Dixon, S. Y. Schwartz, J. I. Walter, M. Protti, V. Gonzalez, J. Biggs, M. Thorwart, W. Rabbel, A tremor and slip event on the Cocos-Caribbean subduction zone as measured by a global positioning system (GPS) and seismic network on the Nicoya Peninsula, Costa Rica. *J. Geophys. Res.* **115**, B10408 (2010).
40. A. G. Wech, K. C. Creager, A continuum of stress, strength and slip in the Cascadia subduction zone. *Nat. Geosci.* **4**, 624–628 (2011).

41. Y. Ito, R. Hino, M. Kido, H. Fujimoto, Y. Osada, D. Inazu, Y. Ohta, T. Iinuma, M. Ohzono, S. Miura, M. Mishina, K. Suzuki, T. Tsuji, J. Ashi, Episodic slow slip events in the Japan subduction zone before the 2011 Tohoku-Oki earthquake. *Tectonophysics* **600**, 14–26 (2013).
42. D. J. Andrews, Rupture velocity of plane strain shear cracks. *J. Geophys. Res.* **81**, 5679–5687 (1976).
43. S. Das, K. Aki, A numerical study of two-dimensional spontaneous rupture propagation. *Geophys. J. Int.* **50**, 643–668 (1977).
44. B. Shibazaki, Y. Iio, On the physical mechanism of silent slip events along the deeper part of the seismogenic zone. *Geophys. Res. Lett.* **30**, 1489 (2003).
45. M. J. Ikari, C. Marone, D. M. Saffer, A. J. Kopf, Slip weakening as a mechanism for slow earthquakes. *Nat. Geosci.* **6**, 468–472 (2013).
46. J. J. Thordsen, W. C. Evans, Y. K. Kharaka, Geochemistry of formation fluids from the SAFOD wells, Parkfield, California, AGU Fall Meeting, San Francisco, CA, 13 to 17 December 2010.
47. M. L. Blanpied, C. J. Marone, D. A. Lockner, J. D. Byerlee, D. P. King, Quantitative measure of the variation in fault rheology due to fluid-rock interactions. *J. Geophys. Res. Solid Earth* **103**, 9691–9712 (1998).
48. C. DeMets, R. G. Gordon, D. F. Argus, S. Stein, Effect of recent revisions to the geomagnetic reversal time scale on estimates of current plate motions. *Geophys. Res. Lett.* **21**, 2191–2194 (1994).
49. S. Miyazaki, K. Heki, Crustal velocity field of southwest Japan: Subduction and arc-arc collision. *J. Geophys. Res.* **106**, 4305–4326 (2001).
50. S. J. Titus, C. DeMets, B. Tikoff, New slip rate estimates for the creeping segment of the San Andreas Fault, California. *Geology* **33**, 205–208 (2005).

Acknowledgments: We thank C. Marone and an anonymous reviewer for helpful reviews. This research used samples and/or data provided by the Ocean Drilling Program, Integrated Ocean Drilling Program, and the International Continental Drilling Project. **Funding:** This work was supported by Deutsche Forschungsgemeinschaft (grants EXC309/FZT15, IK107/1-1, and IK107/3-1) and by the European Research Council under the European Union's Horizon 2020 research and innovation programme (grant 714430). **Author contributions:** M.J.I. conducted friction experiments and data analysis; M.J.I. and A.J.K. planned and wrote the manuscript. **Competing interests:** The authors declare that they have no competing interests. **Data and materials availability:** All data needed to evaluate the conclusions in the paper are present in the paper and/or the Supplementary Materials. Additional data related to this paper may be requested from the authors.

Submitted 20 April 2017
Accepted 31 October 2017
Published 22 November 2017
10.1126/sciadv.1701269

Citation: M. J. Ikari, A. J. Kopf, Seismic potential of weak, near-surface faults revealed at plate tectonic slip rates. *Sci. Adv.* **3**, e1701269 (2017).

Science Advances

Seismic potential of weak, near-surface faults revealed at plate tectonic slip rates

Matt J. Ikari and Achim J. Kopf

Sci Adv **3** (11), e1701269.
DOI: 10.1126/sciadv.1701269